



Research paper

A Novel Classification and Diagnosis of Multiple Sclerosis Method using Artificial Neural Networks and Improved Multi-Level Adaptive Conditional Random Fields

Seyedeh Razieh Mahmoudinejad Dezfouli^{1*}, Yones Kiyani², and Seyed Ataddin Mahmoudinejad Dezfouli³

1. Department of Computer Engineering, Islamic Azad University, Dezfoul Branch, Dezfoul, Iran.

2. Department of Computer Engineering, Islamic Azad University, Central Tehran Branch, Tehran, Iran.

3. Medical Physics and Biomedical Engineering Department, Tehran University of Medical Sciences, Tehran, Iran.

Article Info

Article History:

Received 03 April 2021

Revised 24 July 2021

Accepted 27 November 2021

DOI:

10.22044/JADM.2021.10647.2201

Keywords:

Image Segmentation, Automatic Detection, Multiple Sclerosis, Adaptive Multi-Level Conditional Random Fields (AMCRF), Artificial Neural Network.

* Corresponding author:
rose_mahmudi@yahoo.com (S.R. Mahmoudinejad Dezfouli).

Abstract

Due to the small size, low contrast, and variable position, shape, and texture of multiple sclerosis lesions, one of the challenges of medical image processing is the automatic diagnosis and segmentation of multiple sclerosis lesions in magnetic resonance images. Early diagnosis of these lesions at the first stages of the disease can effectively diagnose and evaluate the treatment. Also automated segmentation is a powerful tool to assist the professionals in improving the accuracy of the disease diagnosis. In this work, we use the modified adaptive multi-level conditional random fields and the artificial neural network in order to segment and diagnose multiple sclerosis lesions. Instead of assuming the model coefficients as constant, they are considered as the variables in the multi-level statistical models. This work aims to evaluate the probability of lesions based on the severity, texture, and adjacent areas. The proposed method is applied to 130 MR images of the multiple sclerosis patients in two test stages, and results in a 98% precision. Also the proposed method reduces the error detection rate by correcting the lesion boundaries using the average intensity of neighborhoods, rotation invariant, and texture for very small voxels with a size of 3-5 voxels, and it shows very few false-positive lesions. The suggested model results in a high sensitivity of 91% with a false positive average of 0.5.

1. Introduction

Magnetic resonance imaging is a key instrument for detecting brain lesions and plaques in the white tissue. The features like high accuracy in detecting soft tissue and distinguishing between normal and abnormal tissue make MR images play a key role in diagnosing MS [1, 2, 6, 11]. Also the MRI techniques can help determine the size and location of the plaques. The main goal of image segmentation is to divide an image into the segments where the pixels of each segment have the most similar features and characteristics. Even for a specialist, it is challenging to perform an accurate evaluation and segmentation of MS

lesions in the MR images [16, 9]. Routine pathology segmentation is difficult for the lesions with small size, location or tissue. Sometimes the lesions reach 3 or 4 small voxels in size. Besides, a low contrast between the target and the background will increase the challenges such as not recognizing the structure or improper labeling [7]. Currently, image segmentation is done manually in order to determine the size and location of lesions. Auto-segmentation can overcome the disadvantages of manual segmentation of images. It is not time-consuming, and performs more accurately than the manual

diagnostics. Another problem of manual diagnostics is counting lesions, considering the confluent lesions, which overlap and cannot be easily separated [1].

The techniques based on the area or textures have been presented. Different segmentation and classification methods have been proposed for the lesion's diagnosis; in most of them, the image pixels are exclusively classified with no regard to the neighboring pixel's spatial association, which makes the small based-voxel lesions classification incorrect [1, 16, 17]. Considering this limitation, a method called GMM-EVT aimed at identifying the white matter lesions has used the farthest point value theory to consider the natural brain tissue model. The advantage of this technique is that all the segmented structures are topologically constrained, allowing subsequent processing such as the cortical unfolding or diffeomorphic shape analysis technique [22]. A new technique by [3] has called LST using a modified mathematical expectation-maximization algorithm to segment the brain tissues and a partial volume class. The limitation of such a technique is that it may converge too late. The segmentation-based atlas requires a pre-segmentation atlas construction. Besides, the trained dataset requires a prior segmentation, and suffers from low or internal variability disadvantages. This method is not flexible, with no limitations on the imaging parameters. Another Atlas-based segmentation method called Lesion-TOADS uses a statistical atlas that can topologically constrain all the segmental structures, and consequently, identify the exact cortical shape due to a subsequent processing. In the small structures of false voxels, the FP rate is increased. Thus the challenge of small-scale lesions remains [17]. Another method called MSmetrix is an accurate automated method for lesion segmentation in MR images with no training data, and is not dependent on the scanner. Although the dice similarity index for MSmetrix is significantly higher than LST, Lesion-TOADS, when there is a large amount of data, the method requires time and the expert knowledge for manual labeling [14]. Several methods such as fuzzy and non-fuzzy clustering techniques are used for the MR image segmentation [8]. Many of these approaches focus on dividing a central object or a healthy structure of surrounding tissue and backgrounds, which often can result in extracting high features based on the intensity and texture patterns from the surrounding background [15]. Some methods use color information, graphical models, and different color spaces. Although the color-based methods have a

relatively worthy speed, their accuracy is not significant [1, 12]. In the recent studies, the researchers have been focusing on the artificial neural network as well as deep learning in order to overcome the challenges and improve the segmentation accuracy of the small voxels [1, 12, 23]. One of the most common DL methods is the convolutional neural networks for detecting lesions in images [2]. A study using CNN for image segmentation seeks to identify the areas of the brain affected by lesions with higher intensity areas. The main advantage of using CNN is the ability to transfer this architecture onto the hardware; however, the issue of the time complexity will remain. Since the method uses fluid-attenuated inversion recovery images, MS lesions appear severe in the FLAIR images; however, their intensity characteristics overlap with the WM and GM textures, causing specific segmentation problems, and are also affected by noise [5, 11]. Some longitudinal approaches based on CNNs independently provide a cross-sectional segmentation of lesions at each time point using longitudinal information. A new model combines the intensity-based and deformation-based features within an end-to-end DL approach, and deals with lesion changes in the brain MRI. The results obtained indicate that the end-to-end training model increase the accuracy of the new T2-w lesion detection [22]. Also the techniques used in a combination of deep CNN and wavelet transform can enable the reduction of image size and highlight the specificity of MS lesions in addition to reducing the number of network parameters. They can perform a better segmentation of the lesions of different sizes. However, the limitation of a high execution time remains [2,3]. Another study uses a sequence of two CNN for automated spinal cord and MS lesion segmentation. The lesion segmentation results are generally within the range of manual segmentations, although the FP rate is not significant and requires further investigation [13]. In a similar study, the DL used with conventional MRI identifies enhanced lesions in MR images from unenhanced multi-parametric MRI with moderate to high accuracy; however, there are a lot of limitations that show that the method needs more investigations for identifying enhancing lesions [20].

Generally, one of the challenges of using the DL methods is the selection of the model and hardware resources. Also the development of a DL method to detect MS lesions in MR images requires more images and experience. Another challenge is that there is no access to adequate

hardware resources to implement the DL architectures [1, 23]. In a study, a statistical hybrid model has diagnosed MS lesions in MR images using the color and texture features. A voxel-based CRF is used to identify the candidate areas. A CRF with higher texture-level features is used to reduce and eliminate the artifacts. This technique has eliminated many of the segmentation challenges [15]. Also it can be improved to reduce false positives in small voxel pathologies, and correct the lesion boundaries by considering the unique features of the image.

The main purpose of this work is to overcome the time complexity limitations, and to improve the accuracy and lesion boundary correction. Also this paper considers the usefulness of feature extraction by modified CRF and explores the use of ANN for automatic feature extraction. Thus this work seeks to address the evaluation of the likelihood of lesion based on severity, tissue, and adjacent areas and the correction of lesion boundaries, accuracy improvement, and the FPs reduction in small voxels by combining a modified CRF with the ANN extracting unique features of the image. The algorithm has two steps to extract higher features of the image. A modified CRF uses higher features of the image such as the average intensity of neighborhoods, rotation invariant, and texture which have been used to segment the images and identify the initial candidate regions. Then ANN uses these candidate regions to automatically extract the features of the image to remove the artifacts and identify the final lesions.

In the following section, in the materials and methods, the CRF and the proposed modified two-phase method are studied. In Section 3, the proposed method used in this work is introduced. Section 4 shows the results and discussion and introduces the database.

2. Materials and Methods

In general, the automatic segmentation strategies of MS lesions are divided into two categories; supervised and unsupervised. In the supervised methods, the information from physician-mediated images and also atlas information is used, and in the unsupervised methods, lesions are segmented directly and without the training step. [16]. In this work, an adaptive CRF model that has been used in [15] is improved by combining the higher-order features, which increases the accuracy of image segmentation. CRFs are one of the most powerful graphical models that include interlocking models. CRFs directly model the likelihood distribution of the label on the

observation condition. They do not include the generating models' defects, which share the label's distribution and observations assuming that the observations are independent from the label's condition.

2.1. Adaptive Multi-level Conditional Random Fields

Suppose that we have two sets of variables X and Y . Consider that we have a graph whose variables are defined on it, i.e. $Y = (Y_v)_{v \in V}$ is a pair (X, Y) that is a random field that has the Markov characteristic below:

$$p(Y_v | X, Y_w, w \neq v) = p(Y_v | X, Y_w, w \square v) \quad (1)$$

in which $w \sim$ and v mean that w and v are in the same neighborhood.

The general conclusion of a random condition is difficult to calculate. However, for some special circumstances, they can be solved simpler:

If the graph is without a loop, then the message passing the algorithms will get the correct answer. In a special case, if the graph is a chain, then the forward-backward algorithm and the Viterbi algorithm get the right answer.

In the case where the graph has binary potentials, the minimum cutting algorithm obtains the optimal answer.

The method of analyzing the AMCRF model is that x and y are represented in sequence, respectively, as the input images and labels, and each image contains the p voxel. The CRF model with Gibbs probability distribution is as follows:

$$p(X | Y) = \frac{1}{Z(x)} \exp(-E(Y | X; \lambda)) = \quad (2)$$

$$\frac{1}{Z(X)} \exp(-\sum_{c \in C} \lambda_c E(Y_c | X))$$

where energy $E(y_c | X) > 0$ is configured for Y_c ; $(y_c | X)$ is the response parameter; $z(x)$ is a segmentation function. C is the set of all clicks in a unidirectional graph and is also a subset of vertices in which both vertices in this subset are represented by an edge connected. E is the graph energy that can be decomposed inside the energy of the clicks. Y_c represents the standard click tag. The most classifying medical vision problems or imaging are related to formulating with the CRF energy clicks [15].

2.2. Modified AMCRF

2.2.1 Voxel-based CRF

This level of CRF with cliques of size up to three is used in order to identify the candidate areas, which is calculated using the following corresponding posterior:

$$P^v(Y|X, \lambda^v, S_v) = \frac{1}{Z(X)} \exp(-E^v(X, Y; \lambda^v, S_v)) = \quad (3)$$

$$\frac{1}{Z(X)} \exp\left[-\left(\sum_{i=1}^n \lambda_\phi^v \phi(y_i | x_i) + S_v \sum_{(i,j) \in N_v} \lambda_\phi^v \phi(y_i, y_j | x_i, x_j) + \sum_{i \in N_{(c)}} \lambda_\delta^v \delta_2(y_i | y_i) + S_v \sum_{(i,j,k) \in N_v} \lambda_\psi^v \psi(y_i, y_j, y_k | x_i, x_j, x_k)\right)\right]$$

where ϕ , ϕ , and ψ represent the voxel surface potentials for the unary, and pairwise and triplet cliques, respectively. The voxel-level parameters, λ_v , modulate each term's effect in the final decision, and are learned in the training phase. The main goal of this level is to evaluate the likelihood of lesion, based on severity, tissue, and adjacent areas, and to improve the lesion boundary correction in the next level. Not all of these detected regions are enhancing lesions, and there are some FPs. A patch p is considered around each candidate. The classification at the voxel level in this work was taken from [15], with some differences. This work improved the voxel-based model, and considered the average intensity parameter of the voxels for just pairwise and triplet cliques to improve the lesion boundaries in the next level. μ and σ are the mean and median for the standard deviation of the patch relatively. Then for each voxel, it calculates the average intensity of the neighborhood, and finally, creates a score S_v as:

$$\mu_v = \frac{1}{N_v} \sum_{k=1}^N i_k \quad (4)$$

$$S_v = \frac{1}{|P|} \sum_{P \in p} (\mu_v, \mu_p) \quad (5)$$

$$\delta(\mu_v, \mu_p) = \begin{cases} 1, & \text{if } \mu_v - \mu_p \geq \sigma \\ 0, & \text{otherwise} \end{cases} \quad (6)$$

$|P|$ is the cardinality of the patch category. Each classification can use Equation (3) for probability. At the end of the voxel level analysis, the probability of lesion per voxel was determined by a binary threshold label (0 or 1). At this point, the goal was to maintain a high sensitivity to the cost of additional FPs [15]. The candidate areas were detected as 26-connectedness in a 3D set of voxels.

Another difference between the method in this research work with [15] is the classifier to model the probabilities. This method uses a Naïve Bayes classifier, which has better results, and is computationally efficient both during the training and testing, and also provides the probabilistic

outputs. The region inside the patch was forwarded to the next level.

2.2.2. Lesion-based CRF: Modified AMCRF with Higher-level Features

At the lesion level, for the region inside the patch where the higher-order textural descriptors are used together with the voxel-wise interactions, a new CRF model is built in order to modify the boundaries of lesions and discriminate the enhancing lesions from the candidates. Concurrently, as the adaptive adjustment possibility of the region boundaries uses separate parameters, considering the τ_k k th texture type and a higher-order $H_p^{\tau_k}$ specificity extracted from the patch area, the modified AMCRF lesion surface is as follows:

$$P^p(Y|X, \lambda^p) = \frac{1}{Z(X)} \exp(-E^p(X, Y; \lambda^p)) = \quad (7)$$

$$\frac{1}{Z(X)} \exp\left[\left(\sum_{i=1}^n \lambda_\phi^p \phi(y_i | x_i) + S_v \sum_{(i,j) \in N_v} \lambda_\phi^p \phi(y_i, y_j | x_i, x_j) + \sum_{i \in N_{(c)}} \lambda_\delta^p \delta_2(y_i | y_i) + S_p \sum_{(i,j,k) \in N_v} \lambda_\psi^p \psi(y_i, y_j, y_k | x_i, x_j, x_k)\right)\right] +$$

$$\sum_{i \in N_v} \lambda_{\Psi_k}^p \Psi_k(y_i^i | H_p^i) +$$

$$\sum_{i=1}^n \lambda_{\Omega_k}^p \Omega_k(y_i, \lambda_i^i | H_p^i) +$$

$$\mu_2(Z) + \mu_3(Z) + U + R + \frac{1}{|P|}$$

A binary variable $y_p^{\tau_k}$ was defined for each higher-order feature $H_p^{\tau_k}$. Ψ_k and Ω_k represent the higher-order unary and pairwise term score responding to the k th texture, and are defined as:

$$\Psi_k(y_p^{J_k} | H_p^{J_k}) = -\log P(y_p^{J_k} | H_p^{J_k}) \quad (8)$$

$$\Omega(y_i, y_p^{J_k} | H_p^{J_k}) = \begin{cases} -\log P(y_p^{J_k} | H_p^{J_k}) \\ -\log(1 - P(y_p^{J_k} | H_p^{J_k})) \end{cases} \quad (9)$$

where $P(y_p^{\tau_k} | H_p^{\tau_k})$ represents the likelihood of detecting a pathology inside the patch, and is obtained by a weighted sum of the probabilities. In addition to the 2D histogram encoding spatial and intensity information in a particular reference pixel and the 2D histogram descriptor that encodes spatial information and gradient orientations [16], this modified method used the statistical moments of the gray-level histogram for feature extraction. Let z be a random variable denoting the image gray levels and $p(z_i)$ $i = 1, 2, \dots, L-1$ be the corresponding histogram, where L

represents the distinct grey levels. $P(z_i)$, $i = 1 \dots N$ is the normalized histogram so that $\sum N_i = 1$ $p(z_i) = 1$. The considered features, extracted from the histogram, are uniformity, intensity variation R , and 2th/3th-order momentum:

$$\mu_2(z) = \sum_{i=0}^{L-1} (z_i - m)^2 p(z_i) \quad (10)$$

$$\mu_3(z) = \sum_{i=0}^{L-1} (z_i - m)^3 p(z_i) \quad (11)$$

$$U = \sum_{i=0}^{L-1} p^2(z_i) \quad (12)$$

$$R = 1 - \frac{1}{1 - \sigma^2(z)} \quad (13)$$

3. Proposed Method

This paper first presents a modified AMCRF model for the segmentation stage and ANN for diagnosing MS in the MR images. In this work, in order to eliminate false lesion areas, a new algorithm has been proposed that maximizes the average segmental results of the physician's segmentation. The detection and segmentation process of MS lesions presented in this section consists of four general blocks depicted in Figure 1. Each one of the blocks is described completely.

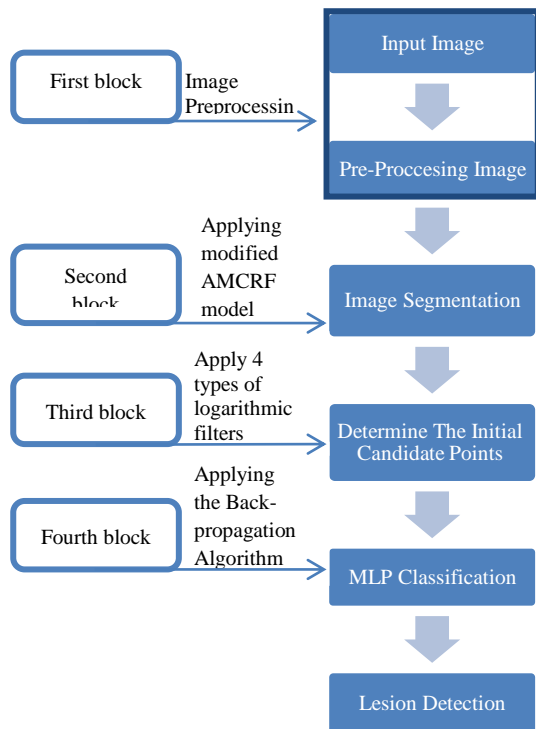


Figure 1. Diagrams of the proposed method (MAMCRF-BPNN).

3.1. First Block-Pre-Processing Image

The pre-processing step was performed on the initial MR image in order to prepare the model for the segmentation step, and the median low-pass filter was applied to enhance the MR image. The

edge filter was used to identify the edges of the regions in the image. Usually MRIs have high dimensions, which make computational challenges for processing. Therefore, the dimensions of the image were adjusted. Before the image segmentation, the border was plotted, and the image was zoned to obtain the image areas. Then the different regions derived from the image were calculated and stored. Finally, the extra obtained areas were eliminated (Figure 2).

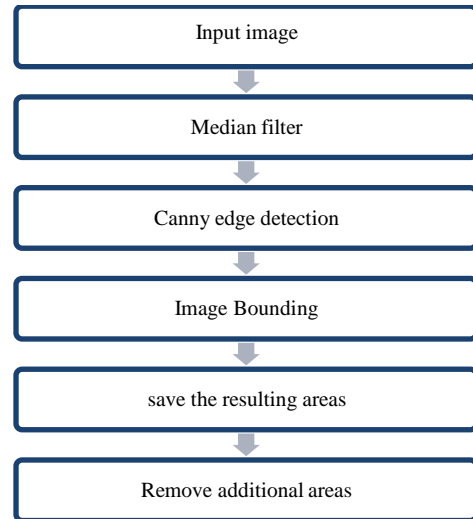


Figure 2. First block Diagram-Pre-processing the image

3.2. Second Block-segmentation of MR Image

Image segmentation was accomplished by a modified adaptive CRF; alongside, the MS lesions in the brain (where the lesion and healthy tissue are connected, such as blood vessels) were segmented. In this block, a modified CRF was used, and the essential areas were taken according to the pixel brightness intensity. At this stage, an initial threshold was made, and the pre-processed image became normal. In the next step, the critical areas were stored. Finally, these areas were labeled. After pre-processing the image, a modified AMCRF was presented in two steps by combining the higher-order features in order to detect and segment the images. In the first step, a voxel-based CRF was used to identify the candidate areas for the lesion. For the voxel-and lesion-level CRF, the method was applied to learn the parameters separately. The standard maximum log-likelihood (or minimum negative log-likelihood-NLL) approach was applied. For learning the modified model phase, the maximum log-likelihood (minimum negative log-likelihood-NLL) was applied in order to find the optimum parameters at each level for M training samples. By applying the voxel-level model to a subset of the training data, a set of lesion candidates was

obtained. According to the true or false detection, the textural features were computed for each candidate and saved, and once the parameters were learned, the task of inference was to compute the joint distribution of all the output variables. Finding the most likely configuration could then be applied to find the labelling that maximized the joint distribution of the output variables.

At this stage, the regions obtained were stored in the SEG matrix. Also there were artifact points at this stage. In the second phase of this algorithm, the lesion level CRF was performed in order to remove the areas mistakenly identified as the lesion candidates.

This model considered the combination of higher-order features for extracting the features. Also differentiation between the healthy and non-healthy tissues was performed (Figure 3).

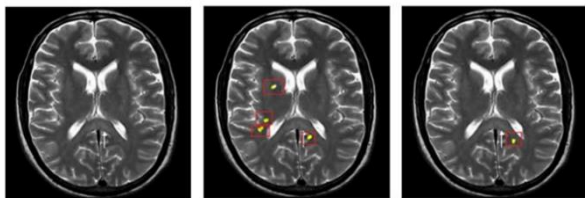


Figure 3. Examined images for modified adaptive MCRF.

In the first stage, there was a CRF voxel-level to produce the lesion areas, and was performed so that the sensitivity of the diagnosed tissue was done with a high precision. Voxel level's labeling for segmentation and classification (location of the lesion) was used in the second phase. In the second stage, a small number of lesion candidates remained. Unlike the previous methods, which only detect the lesions' range, the comparative modified AMCRF model identifies the unnecessary false diagnoses and the extent of the lesion. At this stage, both the healthy voxels and the high-order features were used to optimize and deduce the lesion area (Figure 4).

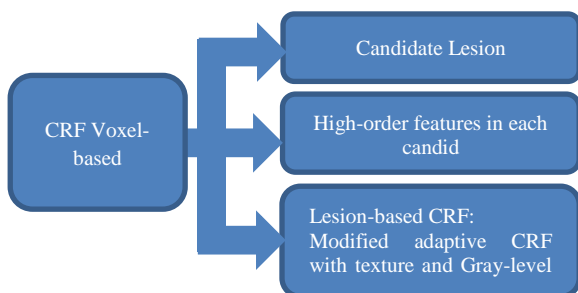


Figure 4. MAMCRF Diagnostic Diagram.

AMCRF: The level of voxel and lesion, as shown in Figure 5, shows how the model automatically uses learning.

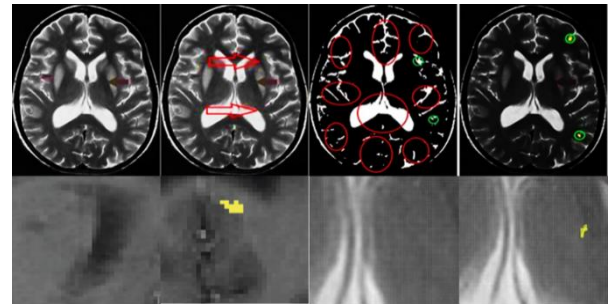


Figure 5. Determination of lesion using multi-level and voxel-level analysis.

Modified voxel-level CRF: At this level, the voxel-based CRF, with voxels of up to 3, was used to identify the candidate area of the lesion, according to Figure 6.

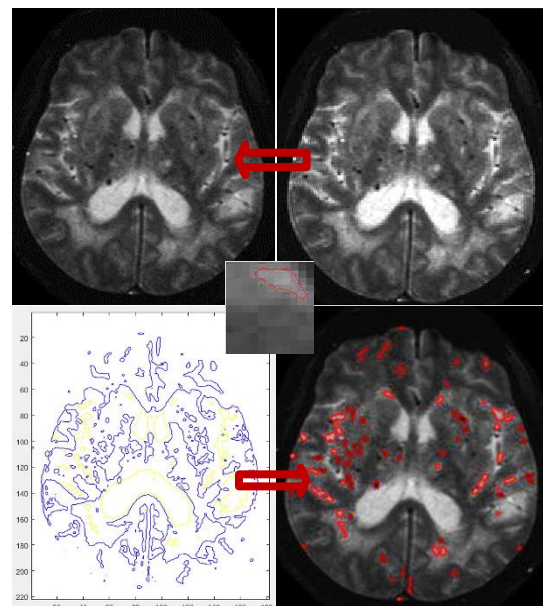


Figure 6. Tested images from the BrainWeb database.

There are multiple probabilities for the possibility of different labels for the neighbouring voxels, which is particularly useful for a small size detection. In cases where the neighbouring voxels have the same label, the field energy will not increase. In the voxel level analysis, there is a possibility of obtaining a lesion. In general, this block's output is the segmental image and the areas of the specified lesion. The candidate regions, as well as the higher-order tissue features, were identified for the MS lesions.

3.3 Third Block-determine Initial Points

Since there's the possibility of existence of artifacts after applying the improved CRF model, and also lesions with small size and large numbers for classification in the neural network results in computational complexity, thus in order to improve the detection accuracy, reduce the computational complexity, and reduce the artifacts, four types of spatial filtering were designed logarithmically in order to detect new target areas, filter and extract the areas suspected to the lesion, and separate the lesion area from unnecessary false diagnoses (derived from the second phase of CRF). The target locations were circular and bright, where the intensity of the signal was relatively different. The filtering included the parts that were not considered to be lesions. At this stage, the initial candidate points were obtained.

3.4. Fourth Block-classification and Diagnosis of MS

In this block, after determining the candidate's initial points, the candidate lesions were inserted into ANN, and the output was the final lesions resulting from MS. In this research work, back-propagation learning was used. The applied neural network had the following structure:

- An input layer was provided to obtain the primary candidate locations with the number of neurons equal to the initial candidate locations. (hyperbolic tangent function).
- 10 neurons for the hidden layer (hyperbolic tangent function).
- An output layer was also considered; the number of neurons in this layer was equal to the number of final lesions (and target position lesions; linear activation function).

The supervised learning was done by a neurologist during the training phase, and a set of patterns were the inputs, and a collection of patterns corresponding to the target position (target) were the outputs of ANN. In the proposed method, the network explores feature extraction automatically. The inputs are the candidate points of the third block, brightness average, and multiply the index area by the brightness value. It is important to note that the lesions are both different in intensity and within the indicator area. However, in the non-lesion areas, these parameters are absent. The third input is relatively long-lived due to lesions whose light intensity is slightly lower in the indicator area. ANN is trained by 1000 epochs and a significant output classifier based on the discovery of the collective characteristics using the data labelled by the MS

specialist in the training phase. An input layer was provided to obtain the primary candidate locations with the number of neurons equal to the initial candidate. An output layer was also considered; the number of neurons in this layer was the same as the number of final lesions. The learning rate was proportional (averagely 0.5). In the hidden layer of this network, ten neurons were considered. In this layer, the hyperbolic tangent function¹ was used. The tanh function was extensively used than the sigmoid function since it delivered a better training performance for the multi-layer ANN. Also it produced a zero-centered output, thereby, supporting the back-propagation process. In Figure 7, the NN diagram block is shown. Finally, the initial image is placed transparently, behind the final output image, to compare two images and the lesion area in the final image.

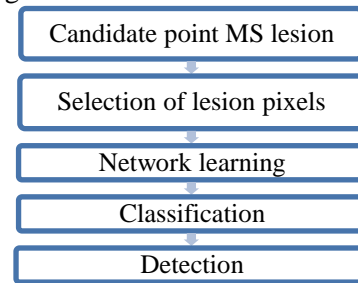


Figure 7. Classification and diagnosis of lesion block diagram.

4. Results and Discussion

In this section, the proposed method is discussed, and the results obtained are compared with the previous techniques. The BrainWeb database contains 130 cases of patients referring to the MS disease with an accuracy of 3 Tesla and also the smallest structural component of $0.5 * 0.5 * 0.5$, with 25 patients' MRIs as a test sample determined by a specialist. The images used for the test dataset included the lesions in different areas from the white matter² of the brain [25]. Each acquisition consisted of five sequences: T1 images before and after contrast with T2, proton density³, and FLAIR. Each sequence is a non-isotropic 3D volume containing 3 mm thick axial slices with a 1 mm * 1 mm intra-plane resolution. The voxel-wise observation vector x consists of the above five MRI modalities intensity, the spatial location of each voxel, and three tissue priors: WM, partial volume, and T2 MS lesion priors.

¹. Hyperbolic Tangent Function (tanh)

². White Matter (WM)

³. Proton Density (PD)

Some were pre-processing on the images including the removal of the non-brain regions of the image, correction for the non-uniformity effects, and bringing MR images into a common spatial and intensity space. There was no need for pre-processing in the training images due to the automatic feature extraction of the back-propagation neural network. For the test images, the WM prior was estimated by registering the ICBM (MNI) average brain atlas to the MR images. The training data used in the proposed MAMCRF included brain MR scans of 1010 cases from several different treatment centers taken from the BrainWeb and NITRC database that were manually labelled amplification lesions [4, 10, 18, 19, 25]. In the proposed model, the lesions were created at different voxel surfaces in different batches, and the model was trained using different classes of training that could help to avoid over-fitting. Three different groups of g_1 , g_2 , and g_3 were considered for train MAMCRF on them. Each batch consisted of 200, 250, and 300 different MR volumes, respectively, resulting in 11×10^6 voxels, 41×10^6 pairs of voxels, and 27×10^6 triplets of voxels. Eventually, these candidate lesions' output was used for tissue stratification. In this work, 45 images of 130 MRIs were used to train the ANN, and 25 MRIs were taken as a test specimen determined by the specialist evaluated for the NN testing. The images are from all the four resonance image types. The 2016 MATLAB was used in a system with a 1.7 GHz processor for simulation and implementation. In Figure 8, the sample images are shown from the database. In the following, Figure 9 shows the lesions detected by the specialist. As shown in Figure 10, the initial and

For a separate image processing evaluation without affecting the noise images (e.g. low-quality images due to configuration errors) or internal faults of the reference methods, the images were specified using the proposed method for TP, FP, TN, and FN metrics. The results obtained were evaluated and compared with the reference values. The pixels marked as references were also provided. Also the pixels detected by the algorithm were TP in white and FN in red (Figure 11). Comparing the reference and extended version of the algorithm detection could help a better evaluation. Since a small displacement could exist between the detected elements and the related reference items, this deviation was necessary. The discovery of the false positive pixels indicated in red was performed.

final locations after implementation were determined.

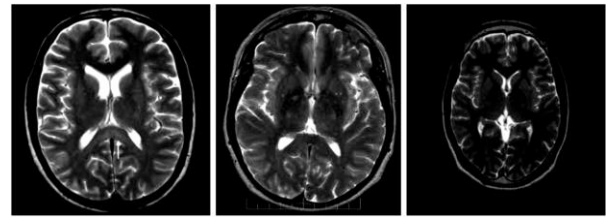


Figure 8. MR images of patients.

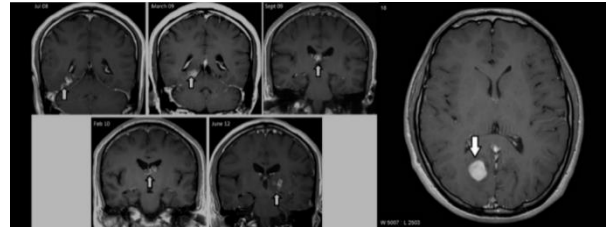


Figure 9. MS lesions on images.

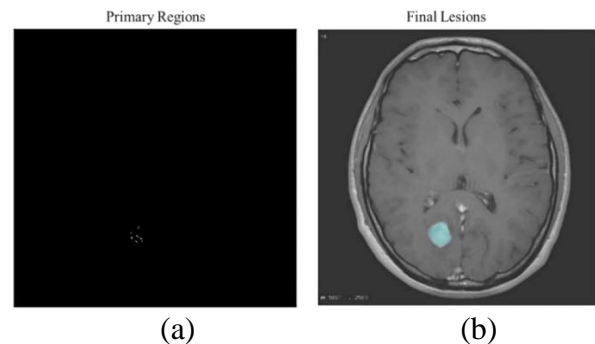


Figure 10. Places a) primary and b) final.

The proposed method was investigated by some metrics. In this research work, the average number of lesions caused by MS in each image was 3.85, ranging from 1 lesion to 12 lesions in an image. At the end of the segmentation phase, an average of 6.49 artifact lesions was found, ranging from 2 to 15 in each image. In the second phase and after training ANN, the artifact numbers were reduced to an average of 0.34 (Table 1).

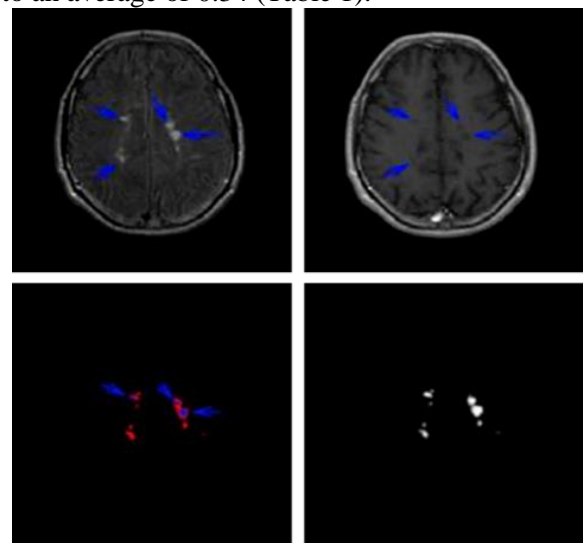


Figure 11. Identification of pixels in white and red (FLAIR image and T1-Weighted).

Table 1. Average number of lesions.

Total number of lesions according to expert segmentation	Average number of lesions per image	Segmentation stage	Neural network stage	TN	AvgFP
113	3.85	6.49	0.31	12400	0.31

The first metric is the precision that can be expressed as follows: the proportion of pixels correctly classified in each class to the total number of pixels corresponding to that class. The proposed algorithm precision was 0.98705.

The second metric is sensitivity. Sensitivity is defined as the ratio of pixels correctly categorized to the total number of pixels determined by the class with true and predictive positive values. Also the proposed algorithm sensitivity was 0.931623. Another metric is specificity. A test must obtain the true negative rate to the total positive and false positive to calculate the specificity. The specificity for the proposed approach was 0.98374. The recall metric was 0.931623. The Dice coefficient was used to determine the correlation accuracy of the segmentation; it was 0.95853 in total. The different value of dice is calculated in Table 2.

Figure 12 shows a qualitative example of the segmentation results for two identified regions. Besides, an image from the T1w type before contrast is shown. Applying the proposed method, TP voxels from these two lesions have resulted, while both cases have remained FPs due to the over-segmentation.

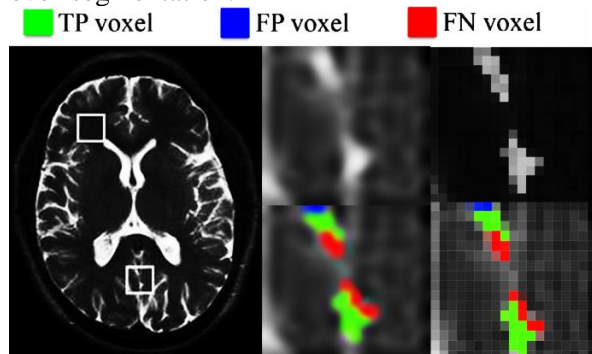


Figure 12. Segmentation results of enhanced lesions from a patient. The T1w image after contrast is shown in (a), where each enhanced lesion is displayed with a square

Compared to the previous methods, the correct number of lesions and the improvement degree is acceptable, and the results of these comparisons can be seen in Tables 2 to 4, investigating the proposed algorithm performance in different lesions sizes. In this research work, the proposed approach was investigated in different lesion sizes. The implementation results are shown in

Table 2. A comparison of the FP and TP values shows that the proposed method has a less FP and TP. Also the false detection rate¹ for lesions of 3-5 voxels was estimated to be 0.29, which was 0.63 lower than FDR in [15]. FDR of the proposed method is efficient and shows a better performance.

As shown in Table 3, a comparison between the results of the proposed method with [15] shows that the proposed method has a significant precision. Also the proposed method sensitivity is still better than [15] and some other techniques. In Table 4, the voxel-based segmentation analysis of the detected lesions is compared with three different metrics. The lesion sizes are computed based on manual labeling but only the overall results are shown in the table.

Furthermore, the convergence curve of ANN for the training data is shown in Figure 13. The mean square error was calculated for the iterations until ANN was converged. The confusion matrix is applicable to perform the accuracy of classifiers, and to show the relationship between the outcomes and the predicted classes. The confusion matrix structure includes the rows and the columns that are equal to the predicted class (output class) and the correct class (target class), respectively. Furthermore, the diagonal cells indicate the percentage of the predicted class correctness, while the off-diagonal cells represent the classifier mistakes. Furthermore, the third column and the third row of the confusion matrix determine the accuracy of each predicted and correct class, respectively, and the last bottom-right cell defines the overall precision.

¹. False Detection Rate (FDR)

Table 2. Calculation of different criteria in different sizes of lesion for the proposed method.

Number of voxels	Overall	3-5	6-10	11-20
Metrics	(+ more than 20 voxels)			
TP	109	30	28	27
FP	21	7	3	3
Dice coefficient	0.95853	0.86701	0.91718	0.91493
False discovery rate (FDR)	0.18	0.29	0.26	0.18

Table 3. Comparison of precision, sensitivity, and rate of error detection.

Approaches	Precision	FD R	Sensitivity
Proposed method	0.98	0.18	0.96
CRF [15] (Karimaghloo, Arnold <i>et al.</i> , 2016)	0.88	0.38	0.96
MSmetrix [5] (Cerasa, Bilotta <i>et al.</i> , 2012)	0.83±0.11	0.21	0.57
Lesion-TOADS [21] (Shiee, Bazin <i>et al.</i> , 2010)	0.81	-	0.50
SLIC0 and convolutional neural network [9] (Diniz, Valente <i>et al.</i> , 2018)	-	-	0.78

Table 4. Comparison of Avg. SENS, DICE, and FDR of the proposed method with other methods.

Method	Avg. SENS (voxel-based)	Avg. DICE (voxel-based)	Avg FDR (voxel-based)
[15] (Karimaghloo, Arnold <i>et al.</i> , 2016)	0.96	0.61	0.38
[13] (Gros, De Leener <i>et al.</i> , 2019)	0.59	0.63	-
[24] (Wang, Zhou <i>et al.</i> , 2018)	0.76	0.68	-
[8] (Dev, Jogi <i>et al.</i> , 2019)	0.82	52.47	-
Proposed method	0.96	0.61	0.18

The confusion matrix of the classification is shown in Figure 14. 109 samples were correctly classified as lesions, which represented 41.44% of all 263. Also 124 non-lesion candidates were correctly classified as non-lesions, which represented 47.14% of all data. Furthermore, 21 non-lesion candidates were incorrectly classified as lesions, which represented 7.98% of all the 263 candidates, and similarly, 4 lesion candidates were incorrectly classified as non-lesion, which represented 1.52% of all the candidates.

Additionally, 96.46% of 113 lesion candidate predictions were correct and 3.54% were incorrect. Likewise, 82.66% of 150 non-lesion predictions were true, and 17.34% were false. Also 86.00% of 113 lesion candidates were correctly predicted as lesion, while 14% were predicted as non-lesion. 96.47% of 150 non-lesion candidates were correctly classified as non-lesion, and 3.53% were classified as the lesion. Overall, 98.70% of the predictions were correct and 2.30% were wrong.

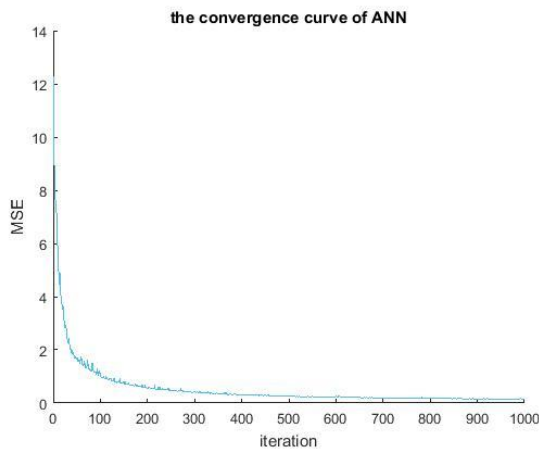


Figure 13. Convergence curve of ANN.

Output Class	Positive 1	109 41.44%	21 7.98%	96.46% 3.54%
	Negative 0	4 1.52%	124 47.14%	82.66% 17.34%
		96.47% 3.53%	86.00% 14.00%	98.70% 2.30%
	Positive 1		Negative 0	
Target Class				

Figure 14. Confusion matrix for the proposed algorithm.

4. Conclusions

The proposed algorithm is concerned with the detection and locating the small structures in MR image pathologies. In this research work, an improved model was proposed for the segmentation and diagnosis of MS lesions in MR images. MAMCRF was combined with the higher-order features in order to detect and analyze the pathology in the first-order graphic model of a voxel-based CRF. Also a new CRF was developed to identify the candidate lesions at the lesion level, and prevent the removal of unknown error areas, which included higher tissue characteristics and analyzing the statistical moments of the gray-level histogram. The average sensitivity of the proposed algorithm was 0.96460, and the precision was 0.98705. Both metrics were better than the prior works. Besides, the specificity value for the proposed approach was 0.98374, which was better than most prior research works. Comparing the proposed algorithm results with the other methods showed that the proposed method was better in detecting the small lesion size and boundaries. On the other hand, using the MAMCRF method in the segmentation step simplifies the detection

boundaries. However, the problem of computational and temporal complexity of the algorithm remains a challenge in this area. For future research works, this new method could be used for a more extensive train image database to achieve better results. Combining the DL techniques with a modified segmentation method could improve the accuracy of lesion diagnosis, and increase the detection rate for small pathologies. Also using the MAMCRF segmentation method could be a practical step in modifying the lesion boundary correction and increasing the speed of the algorithm.

References

- [1] A. Alijamaat, A. NikravanShalmani, P. Bayat, "Multiple sclerosis lesion segmentation from brain MRI using U-Net based on wavelet pooling," *International journal of computer assisted radiology and surgery.*; vol. 16, no. 9, pp. 1459-67, Sep 2021.
- [2] A. Alijamaat, A. NikravanShalmani, P. Bayat, "Multiple sclerosis identification in brain MRI images using wavelet convolutional neural networks," *International journal of imaging systems and technology*, vol. 31, no. 2, pp. 778-85, Jun 2021.
- [3] A. Alijamaat, A. NikravanShalmani, P. Bayat, "Diagnosis of Multiple Sclerosis Disease in Brain MRI Images using Convolutional Neural Networks based on Wavelet Pooling," *Journal of AI and Data Mining*, vol. 9, no. 2, pp. 161-168, Apr 2021.
- [4] M. Cabezas, A. Oliver, E. Roura, J. Freixenet, JC, Vilanova, L. Ramió-Torrentà, À. Rovira, X. Lladó, "Automatic multiple sclerosis lesion detection in brain MRI by FLAIR thresholding" *Computer methods and programs in biomedicine*, vol. 115, no. 3, pp. 147-61, Jul 2014.
- [5] C.A. Cocosco, V. Kollokian, R.K.-S. Kwan, and A.C. Evans: "BrainWeb: Online Interface to a 3D MRI Simulated Brain Database" *NeuroImage*, vol. 5, no. 4, part 2/4, S425, May 1997.
- [6] A. Cerasa, E. Bilotta, A. Augimeri, A. Cherubini, P. Pantano, G. Zito, P. Lanza, P. Valentino, M. C. Gioia, and A. Quattrone, "A cellular neural network methodology for the automated segmentation of multiple sclerosis lesions," *Journal of neuroscience methods*, vol. 203, no. 1, pp. 193-199, Jan 2012.
- [7] A. Chaudhuri, "Multiple sclerosis is primarily a neurodegenerative disease." *Journal of Neural Transmission*, vol. 120, no. 10, pp. 1463-1466, Oct 2013.
- [8] S. Datta, B. R. Sajja, R. He, R. K. Gupta, J. S. Wolinsky, and P. A. Narayana, "Segmentation of gadolinium-enhanced lesions on MRI in multiple sclerosis," *Journal of Magnetic Resonance Imaging: An Official Journal of the International Society for Magnetic Resonance in Medicine*, vol. 25, no. 5, pp. 932-937, May 2007.

- [9] K. B. Dev, P. S. Jogi, S. Niyas, S. Vinayagamani, C. Kesavadas, and J. Rajan, "Automatic detection and localization of Focal Cortical Dysplasia lesions in MRI using fully convolutional neural network," *Biomedical Signal Processing and Control*, vol. 52, pp. 218-225, Jul 2019.
- [10] P. H. B. Diniz, T. L. A. Valente, J. O. B. Diniz, A. C. Silva, M. Gattass, N. Ventura, B. C. Muniz, and E. L. Gasparetto, "Detection of white matter lesion regions in MRI using SLIC0 and convolutional neural network," *Computer methods and programs in biomedicine*, vol. 167, pp. 49-63, Dec 2018.
- [11] D.L. Collins, A.P. Zijdenbos, V. Kollokian, J.G. Sled, N.J. Kabani, C.J. Holmes, and A.C. Evans: "Design and Construction of a Realistic Digital Brain Phantom", *IEEE Transactions on Medical Imaging*, Vol. 17, no. 3, pp.463-468, June 1998.
- [12] P. G. Freire, and R. J. Ferrari, "Multiple sclerosis lesion enhancement and white matter region estimation using hyper-intensities in FLAIR images," *Biomedical Signal Processing and Control*, vol. 49, pp. 338-348, Mar 2019.
- [13] D. García-Lorenzo, S. Francis, S. Narayanan, D. L. Arnold, and D. L. Collins, "Review of automatic segmentation methods of multiple sclerosis white matter lesions on conventional magnetic resonance imaging," *Medical image analysis*, vol. 17, no. 1, pp. 1-18, Jan 2013.
- [14] C. Gros, B. De Leener, A. Badji, J. Maranzano, D. Eden, S. M. Dupont, J. Talbott, R. Zhuoquiong, Y. Liu, and T. Granberg. "Automatic segmentation of the spinal cord and intramedullary multiple sclerosis lesions with convolutional neural networks," *Neuro-image*, vol. 184, pp. 901-915, Jan 2019.
- [15] S. Jain, D. M. Sima, A. Ribbens, M. Cambron, A. Maertens, W. Van Hecke, J. De Mey, F. Barkhof, M. D. Steenwijk, and M. Daams, "Automatic segmentation and volumetry of multiple sclerosis brain lesions from MR images," *Neuro-Image: Clinical*, vol. 8, pp. 367-375, Jan 2015.
- [16] Z. Karimaghloo, D. L. Arnold, and T. Arbel. "Adaptive multi-level conditional random fields for detection and segmentation of small enhanced pathology in medical images," *Medical image analysis*, vol. 27, pp. 17-30, Jan 2016.
- [17] N. K. Kasabov, "NeuCube: A spiking neural network architecture for mapping, learning and understanding of Spatio-temporal brain data," *Neural Networks*, vol. 52, pp. 62-76, Apr 2014.
- [18] P. A. Narayana, Coronado, I., S. J. Sujit, J. S. Wolinsky, F. D. Lublin, and R. E. Gabr, Deep learning for predicting enhancing lesions in multiple sclerosis from non-contrast MRI. *Radiology*, vol. 294, no. 2, pp. 398-404, Feb 2020.
- [19] R.K.-S. Kwan, A.C. Evans, and G.B. Pike, "MRI simulation-based evaluation of image-processing and classification methods," *IEEE Transactions on Medical Imaging*, Vol. 18, no. 11, pp. 1085-97, Nov 1999.
- [20] R.K.-S. Kwan, A.C. Evans, and G.B. Pike, "An Extensible MRI Simulator for Post-Processing Evaluation", Visualization in Biomedical Computing (VBC'96). *Lecture Notes in Computer Science*, Springer-Verlag, vol. 1131., pp. 135-140, Sep 1996.
- [21] M. Salem, S. Valverde, M. Cabezas, D. Pareto, A. Oliver, J. Salvi, and X. Lladó, "A fully convolutional neural network for new T2-w lesion detection in multiple sclerosis," *NeuroImage: Clinical*, vol. 25, pp. 102149, Jan 2020.
- [22] N. P.-L. Shiee, A. Bazin, D. S. Ozturk, P. Reich, A. Calabresi and D. L. Pham, "A topology-preserving approach to the segmentation of brain images with multiple sclerosis lesions," *Neuro-Image*, vol. 49, no. 2, pp. 1524-1535, Jan 2010.
- [23] A. Shoeibi, M. Khodatars, M. Jafari, P. Moridian, M. Rezaei, R. Alizadehsani, and U. R. Acharya, "Applications of Deep Learning Techniques for Automated Multiple Sclerosis Detection using Magnetic Resonance Imaging: A Review," *arXiv preprint arXiv*, pp. 2105.04881, Sep 2021.
- [24] R. Wang, C. Li, J. Wang, X. Wei, Y. Li, C. Hui, Y. Zhu, and S. Zhang, "Automatic segmentation of white matter lesions on magnetic resonance images of the brain by using an outlier detection strategy," *Magnetic resonance imaging*, vol. 32, no. 10, pp. 1321-1329, Dec 2014.
- [25] Y. Wang, Y. Zhou, H. Wang, J. Cui, B. A. Nguchu, X. Zhang, B. Qiu, X. Wang, and M. Zhu, "Voxel-based automated detection of focal cortical dysplasia lesions using diffusion tensor imaging and T2-weighted MRI data," *Epilepsy & Behavior*, vol. 84, pp. 127-134, Jul 2018.

یک روش جدید طبقه‌بندی و تشخیص مولتیپل اسکروزیس با استفاده از شبکه‌های عصبی مصنوعی و میدان‌های تصادفی شرطی تطبیقی چند سطحی بهبودیافته

سیده راضیه محمودی نژادذرفولی^{۱*}، یونس کیانی^۲ و سید عطا الدین محمودی نژادذرفولی

^۱ گروه مهندسی کامپیوتر، دانشگاه آزاد اسلامی، واحد دزفول، دزفول، ایران.

^۲ گروه مهندسی کامپیوتر، دانشگاه آزاد اسلامی، واحد تهران مرکز، تهران، ایران.

^۳ گروه فیزیک پزشکی و مهندسی بیومدیکال، دانشگاه علوم پزشکی تهران، تهران، ایران.

ارسال ۲۰۲۱/۰۴/۰۳؛ بازنگری ۲۰۲۱/۰۷/۲۴؛ پذیرش ۲۰۲۱/۱۱/۲۷

چکیده:

یکی از چالش‌های پردازش تصویر پزشکی، تشخیص و تقسیم خودکار ضایعات مولتیپل اسکروزیس در تصاویر تشدید مغناطیسی است. تشخیص زودهنگام این ضایعات در مراحل اولیه بیماری می‌تواند به طور موثری در درمان بیماری کمک دهنده باشد. همچنین تقسیم‌بندی خودکار ابزار قدرتمندی برای کمک به متخصصان در بهبود دقت تشخیص بیماری است. در این مقاله، از میدان‌های تصادفی شرطی چندسطحی تطبیقی اصلاح شده و شبکه عصبی مصنوعی به منظور بخش‌بندی و تشخیص ضایعات مولتیپل اسکروزیس استفاده شده است. در این مدل به جای اینکه ضرایب مدل ثابت فرض شوند، در مدل‌های آماری چند سطحی متغیر در نظر گرفته می‌شوند. هدف از این پژوهش ارزیابی احتمال ضایعات بر اساس شدت، بافت و نواحی مجاور است. روش پیشنهادی بر روی ۱۳۰ تصویر MR از بیماران مبتلا به مولتیپل اسکروزیس در دو مرحله آزمایشی اعمال شده است و دقت ۹۸ درصد را به دست آورد. همچنین روش پیشنهادی با اصلاح مرزهای ضایعه با استفاده از میانگین شدت همسایگی‌ها، چرخش ثابت و بافت برای وکسل‌های بسیار کوچک با اندازه ۵-۳ وکسل، میزان تشخیص خطا را کاهش می‌دهد و ضایعات مثبت کاذب بسیار کمی را نشان می‌دهد. مدل پیشنهادی منجر به حساسیت بالای ۹۱ درصد با میانگین مثبت کاذب ۰,۵ می‌شود.

کلمات کلیدی: بخش‌بندی تصویر، تشخیص خودکار، مولتیپل اسکروزیس، میدان‌های تصادفی شرطی چند سطحی تطبیقی (AMCRF)، شبکه عصبی مصنوعی.